Quantitative Preclinical Imaging of TSPO Expression in Glioma Using *N,N*-Diethyl-2-(2-(4-(2-^{18}F-Fluoroethoxy) Phenyl)-5,7-Dimethylpyrazolo[1,5-*a*]Pyrimidin-3-yl)Acetamide

Dewei Tang[1,2], Matthew R. Hight[1,3], Eliot T. McKinley[1,4], Allie Fu[1], Jason R. Buck[1,5], R. Adam Smith[1,5], Mohammed Noor Tantawy[1,5], Todd E. Peterson[1,2,5,6], Daniel C. Colvin[1,5], M. Sib Ansari[1,5], Michael Nickels[1,5], and H. Charles Manning[1,2,4,5,7,8]

[1]Vanderbilt University Institute of Imaging Science, Vanderbilt University Medical Center, Nashville, Tennessee; [2]Program in Chemical and Physical Biology, Vanderbilt University Medical Center, Nashville, Tennessee; [3]Interdisciplinary Materials Science Program, Department of Physics and Astronomy, Vanderbilt University, Nashville, Tennessee; [4]Department of Biomedical Engineering, Vanderbilt University, Nashville, Tennessee; [5]Department of Radiology and Radiological Sciences, Vanderbilt University Medical Center, Nashville, Tennessee; [6]Department of Physics and Astronomy, Vanderbilt University, Nashville, Tennessee; [7]Department of Neurosurgery, Vanderbilt University Medical Center, Nashville, Tennessee; and [8]Vanderbilt Ingram Cancer Center, Vanderbilt University Medical Center, Nashville, Tennessee

There is a critical need to develop and rigorously validate molecular imaging biomarkers to aid diagnosis and characterization of primary brain tumors. Elevated expression of translocator protein (TSPO) has been shown to predict disease progression and aggressive, invasive behavior in a variety of solid tumors. Thus, noninvasive molecular imaging of TSPO expression could form the basis of a novel, predictive cancer imaging biomarker. In quantitative preclinical PET studies, we evaluated a high-affinity pyrazolopyrimidinyl-based TSPO imaging ligand, *N,N*-diethyl-2-(2-(4-(2-^{18}F-fluoroethoxy)phenyl)-5,7-dimethylpyrazolo[1,5-*a*]pyrimidin-3-yl)acetamide (^{18}F-DPA-714), as a translational probe for quantification of TSPO levels in glioma. **Methods:** Glioma-bearing rats were imaged with ^{18}F-DPA-714 in a small-animal PET system. Dynamic images were acquired simultaneously on injection of ^{18}F-DPA-714 (130–200 MBq/0.2 mL). Blood was collected to derive the arterial input function (AIF), with high-performance liquid chromatography radiometabolite analysis performed on selected samples for AIF correction. Compartmental modeling was performed using the corrected AIF. Specific tumor cell binding of DPA-714 was evaluated by radioligand displacement of ^{3}H-PK 11195 with DPA-714 in vitro and displacement of ^{18}F-DPA-714 with an excess of DPA-714 in vivo. Immediately after imaging, tumor and healthy brain tissues were harvested for validation by Western blotting and immunohistochemistry. **Results:** ^{18}F-DPA-714 was found to preferentially accumulate in tumors, with modest uptake in the contralateral brain. Infusion with DPA-714 (10 mg/kg) displaced ^{18}F-DPA-714 binding by greater than 60% on average. Tumor uptake of ^{18}F-DPA-714 was similar to another high-affinity TSPO imaging ligand, ^{18}F-*N*-fluoroacetyl-*N*-(2,5-dimethoxybenzyl)-2-phenoxyaniline, and agreed with ex vivo assay of TSPO levels in tumor and healthy brain. **Conclusion:** These studies illustrate the feasibility of using ^{18}F-DPA-714 for visualization of TSPO-expressing brain tumors. Importantly, ^{18}F-DPA-714 appears suitable for quantitative assay of tumor TSPO levels in vivo. Given the relationship between elevated TSPO levels and poor outcome in oncology, these studies suggest the potential of ^{18}F-DPA-714 PET to serve as a novel predictive cancer imaging modality.

Key Words: glioma; TSPO; pyrazolopyrimidine; DPA-714; positron emission tomography

J Nucl Med 2012; 53:287–294
DOI: 10.2967/jnumed.111.095653

Malignant gliomas are the most common primary brain tumor and are characterized by invasive growth and recalcitrance to therapy. Currently, diagnosis and grading of gliomas are based on the pathology of resected specimens, with limitations inherent to sampling errors and heterogeneity. Given these limitations, clinical decisions are routinely guided by imaging (*1*). The most common imaging metrics used to detect and diagnose brain tumors are CT and MRI. These modalities provide little, if any, molecular information attributable to the pathologic status of the disease. Furthermore, numerous studies document the inherent difficulty associated with determination of brain tumor extent using CT or MRI, particularly with infiltrative disease. PET using ^{18}F-FDG is an important technique for the detection of brain tumors. However, high glucose uptake in normal brain results in modest tumor-to-background ratios with ^{18}F-FDG, which can confound delineation of disease margins and subsequent grading. Therefore, there is a considerable need to develop and validate improved molecular

Received Jul. 12, 2011; revision accepted Sep. 27, 2011.
For correspondence or reprints contact: H. Charles Manning, Vanderbilt University Institute of Imaging Science (VUIIS), Vanderbilt University Medical School, 1161 21st Ave. S., AA 1105 MCN, Nashville, TN 37232-2310.
E-mail: henry.c.manning@vanderbilt.edu
Guest Editor: Wolf-Dieter Heiss, Max-Planck-Institut fur Neurologische Forschung
Published online Jan. 17, 2012.

imaging techniques suitable for detection or molecular profiling of brain tumors (*2*).

Translocator protein (TSPO), also referred to as peripheral benzodiazepine receptor (PBR), is an 18-kDa protein typically localized to the outer mitochondrial membrane. TSPO participates in the regulation of numerous cellular processes, including cholesterol metabolism, steroid biosynthesis, cellular proliferation, and apoptosis. In normal tissues, TSPO expression tends to be highest in steroid-producing and mitochondrion-enriched tissues such as skeletal muscle, renal tissue, and myocardium, whereas tissues such as liver and brain exhibit comparatively modest expression (*3*). Elevated TSPO expression is found in numerous disease states, including neuroinflammation (*4*) and neurologic disorders such as Alzheimer's (*5*) and Huntington's (*6*) diseases, as well as cancers of the breast (*7,8*), prostate (*9*), oral cavity (*10*), colon (*11–13*), liver (*14*), and brain (*15,16*). Elevated TSPO expression has also been linked with disease progression and diminished survival in patients with oral (*10,17*), colorectal (*11*), breast (*18*), and brain (*19*) cancers. Additionally, elevated TSPO levels appear to be associated with aggressive, metastatic behavior in breast and colorectal cancer (*7,20*). Collectively, these data illuminate TSPO expression as a potentially important prognostic biomarker in oncology and suggest the utility of tumor-selective TSPO PET ligands for cancer imaging.

Recently, a variety of novel TSPO PET ligands have emerged from the literature, including aryloxyanilides, indoleacetamides, pyrazolopyrimidines, and imidazolepyridines (*21*). We recently reported ^{18}F-*N*-fluoroacetyl-*N*-(2,5-dimethoxybenzyl)-2-phenoxyaniline (^{18}F-PBR06) as a high-affinity tracer for visualization of brain tumors and quantification of TSPO expression in tumor and normal tissue (*22*). The goal of the present study was to evaluate another high-affinity TSPO PET ligand, *N,N*-diethyl-2-(2-(4-(2-^{18}F-fluoroethoxy)phenyl)-5,7-dimethylpyrazolo[1,5-*a*]pyrimidin-3-yl)acetamide (^{18}F-DPA-714), in cancer imaging studies. Our data illustrate the feasibility of using ^{18}F-DPA-714 for visualization of TSPO-expressing brain tumors. Importantly, ^{18}F-DPA-714 appears suitable for quantitative assay of tumor TSPO levels in vivo. Given the relationship between elevated TSPO levels and poor outcome in oncology, these studies suggest the potential of ^{18}F-DPA-714 PET to serve as a novel and predictive cancer imaging modality.

MATERIALS AND METHODS

Chemicals and Ligand and Radioligand Precursor Preparation

^{3}H-PK 11195 was purchased from PerkinElmer. Phosphate-buffered saline and CytoScint ES Liquid Scintillation Cocktail were purchased from MP Biomedicals. All synthesis reagents were purchased from Sigma-Aldrich.

^{19}F-DPA-714 (DPA-714) and radioligand precursor were prepared according to published methods (*23*).

In Vitro Radioligand Binding Assay

Radioligand binding experiments were conducted using C6 glioma cell lysates as previously described, using DPA-714 as the cold ligand (*22,24*). All experiments were performed in triplicate.

Radioligand Preparation

^{18}F-DPA-714 was prepared analogously to published methods (*25*). In short, using a commercial apparatus (TRACERlab FX F-N; GE Healthcare), we dried aqueous ^{18}F-fluoride ion (~111 GBq) by iterative cycles of addition and evaporation of acetonitrile, followed by complexation with K^+-K^+-2.2.2/K_2CO_3. The complex was reacted with 4-(3-(2-(diethylamino)-2-oxoethyl)-5,7-dimethylpyrazolo[1,5-*a*]pyrimidin-2-yl)phenethyl 4-methylbenzenesulfonate (3.0 mg) at 165°C for 5 min in anhydrous dimethyl sulfoxide (0.6 mL). ^{18}F-DPA-714 was purified using reversed-phase high-performance liquid chromatography (HPLC) (C18, Dynamax 250 × 21.4 mm; Varian) eluted at 6.0 mL/min with 10 mM NaH_2PO_4 buffer (pH 6.7) and ethanol (47.5:52.5; v/v). ^{18}F-DPA-714 was collected, washed with 120 mL of water (deionized), and eluted from a C18 Sep-Pak (Waters) with ethanol (1.0 mL) into a sterile flask loaded with saline (9.0 mL). Typical specific activities were 418 TBq/mmol or greater.

Rat Model

All studies involving animals were conducted in compliance with federal and institutional guidelines. Two weeks before imaging, healthy male Wistar rats (n = 14) were stereotactically inoculated in the right hemisphere with 1.0×10^5 C6 glioma cells (American Type Tissue Collection). Before imaging, all rats were affixed with venous and arterial catheters.

MRI

MRI was used to localize the C6 tumors. Rats were secured prone in a radiofrequency coil (38-mm inner diameter) and placed in a 4.7-T horizontal bore imaging system (Varian Inc.). A constant body temperature of 37°C was maintained using heated airflow. An initial multislice gradient-echo imaging sequence (repetition time, 150 ms; echo time, 3.5 ms; matrix, 128 × 128; field of view, 40 × 40 mm^2; slice thickness, 2 mm) was used to acquire 7 slices in each imaging plane (axial, coronal, and sagittal) for proper positioning of subsequent scans. A multislice T2-weighted fast spin-echo scan with 8 echoes and 8.0-ms echo spacing (effective echo time, 32 ms) was then collected with a repetition time of 2,000 ms; field of view of 32 × 32 mm^2; matrix of 128 × 128; 16 acquisitions; and 8 coronal slices of 2-mm thickness.

PET/CT

PET/CT was performed within 24 h of MRI in rats with confirmed tumors (n = 14). Tumor-bearing rats were administered ^{18}F-DPA-714 (130–200 MBq/0.2 mL) via a jugular catheter while in a microPET Focus 220 scanner (Siemens). Data were collected in list-mode format for 90 min, followed by a CT scan (microCAT II; Siemens) for attenuation correction. For displacement studies (n = 4), DPA-714 (10 mg/kg) was injected at 30 min via a jugular catheter.

The dynamic PET acquisition was divided into twelve 10-s frames for the first 2 min, three 60-s frames for the following 3 min, and seventeen 300-s frames for the duration of the scan. The raw data within each frame were then binned into 3-dimensional sinograms, with a span of 3 and ring difference of 47. The sinograms were reconstructed into tomographic images (128 × 128 × 95) with voxel sizes of 0.095 × 0.095 × 0.08 cm^3,

after scatter and attenuation corrections were applied, using a 2-dimensional ordered-subsets expectation-maximization algorithm with 16 subsets and 4 iterations. Attenuation correction was accomplished by generating an attenuation map from the CT image. The CT image was first coregistered with the small-animal PET image, segmented, and then projected into sinogram space with a span of 47 and ring difference of 23.

Measurement of ^{18}F-DPA-714 in Plasma

Immediately after administration of ^{18}F-DPA-714, arterial blood samples (50 μL) were collected at 10-s intervals during the first minute of scanning, followed by collection at 90 s and 2, 8, 12, 20, 30, 45, 60, 75, and 90 min. Blood samples (50 μL) were centrifuged at 14,000 revolutions per minute for 5 min in a microcentrifuge. The plasma (15 μL) was then removed and the radioactivity measured in a NaI well counter (Capintec).

HPLC Radiometabolite Analysis

Briefly, arterial blood (200 μL) was collected at 2, 12, 30, 60, and 90 min. After centrifugation, plasma was extracted with acetonitrile:water (340 μL, 7:1, v/v). The mixture was centrifuged and the supernatant used for reversed-phase HPLC analysis with 0.1 M aqueous ammonium acetate (NH_4)OAc (pH 10) and acetonitrile (30:70; v/v) at 1.0 mL/min on a C18 Dynamax 250 × 4.6 mm (Varian) column. Radiochromatographic data were recorded and collected using a radioisotope detector (Bioscan), decay-corrected to time zero of each radiochromatogram, and smoothed using a locally weighted scatterplot method (*26*). The plasma time–activity curve was corrected according to the fraction of unchanged radioligand.

Histology

Whole brains were harvested and fixed in 4% formalin for 48 h, followed by paraffin embedding for immunohistochemistry. Tissue sections of 5.0-μm thickness were taken, and TSPO immunoreactivity assessed using a TSPO-specific rabbit polyclonal antibody, a gift from Professor Vassilios Papadopoulos of McGill University. Immunoreactivity was assessed using a horseradish peroxidase detection kit (Dako). Hematoxylin and eosin staining was used to quantify cell density and tumor localization. For histology quantification, optical density measurements of multispectral image cubes were collected using a CRI Nuance camera, and the total intensity of positive pixels determined as reported previously (*22*).

Image Analysis and Modeling

Time–activity curves were generated by manually drawing 3-dimensional volumes of interest over tumor and contralateral brain using ASIPro (Siemens). The arterial input function (AIF) was computed from plasma sampling during imaging and corrected for metabolism of the parent ligand. Of the 14 animals imaged in this study, data collected from 3 animals were excluded from modeling because of insufficient collection of arterial blood required for AIF determination. Both a 2-compartment, 2-rate-constant kinetic model and a 3-compartment, 4-rate-constant kinetic model were used to characterize ^{18}F-DPA-714 pharmacokinetics with the COMKAT software package. Model fit was determined by inspection. In the 2-compartment, 2-rate-constant kinetic model, we determined model parameters for the influx (K_1) and efflux (k_2) rate constants of the radioligand diffusion between the plasma and tissue compartments. In the 3-compartment, 4-rate-constant kinetic model, we determined model parameters for influx (K_1) and efflux (k_2) and exchange constants between specific binding (k_3) and free ligand (including nonspecific binding) (k_4) compartments for both normal brain tissue and tumor. For the 3-compartment, 4-rate-constant kinetic model, the total volume of distribution (V_T) was then calculated using the equation $V_T = (K_1/k_2)(1 + k_3/k_4)$ for the whole brain (excluding tumor) and for the tumor (*27*). Additionally, using the first 60 min of data (beyond which tracer was undetectable in blood), a graphical analysis method (*28*) was used to estimate the total distribution volume for the whole brain (excluding tumor) and tumor. Analysis of statistical significance employed the Student *t* test (Prism 4.0; GraphPad Software).

RESULTS

Specific Binding of DPA-714 to TSPO in C6 Glioma Cell Line Homogenates

Previous studies explored ^{18}F-DPA-714 within the context of neuroinflammation (*25,29*). Our interest in assaying TSPO expression in glioma led us to evaluate the specific binding of DPA-714 in glioma cell line homogenates (Fig. 1). We found DPA-714 to be highly specific for TSPO, exhibiting robust dose-dependent displacement of the isoquinoline carboxamide ^{3}H-PK 11195 to near-background levels. Nonlinear regression analysis of the binding data yielded an inhibitory concentration of 50% for DPA-714 of approximately 10.9 nM, similar to our previous observations with the aryloxyanilide, PBR06 (*22*).

In Vivo Uptake of ^{18}F-DPA-714 in C6 Glioma

Before PET with ^{18}F-DPA-714, brain tumors were localized using T2-weighted MRI. Similar to previous observations, the C6 tumors exhibited marked hyperintensity indicative of longer T2 relaxation times, compared with surrounding brain (Fig. 2A). Dynamic PET of ^{18}F-DPA-714 illustrated that most of the uptake in the brain was localized to tumor tissue, with only modest accumulation in adjacent, normal areas of the brain (Figs. 2B and 2D). Over the last 30 min of the PET scan, total radioactivity levels in tumor tissue were approximately 4-fold higher

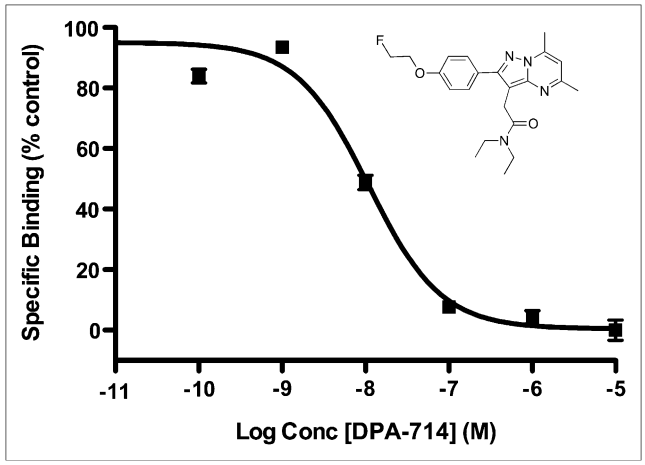

FIGURE 1. Chemical structure of DPA-714 (inset). Radioligand displacement of ^{3}H-PK 11195 using DPA-714 in C6 glioma cell lysate (inhibitory concentration of 50%, 10.9 nM). conc = concentration.

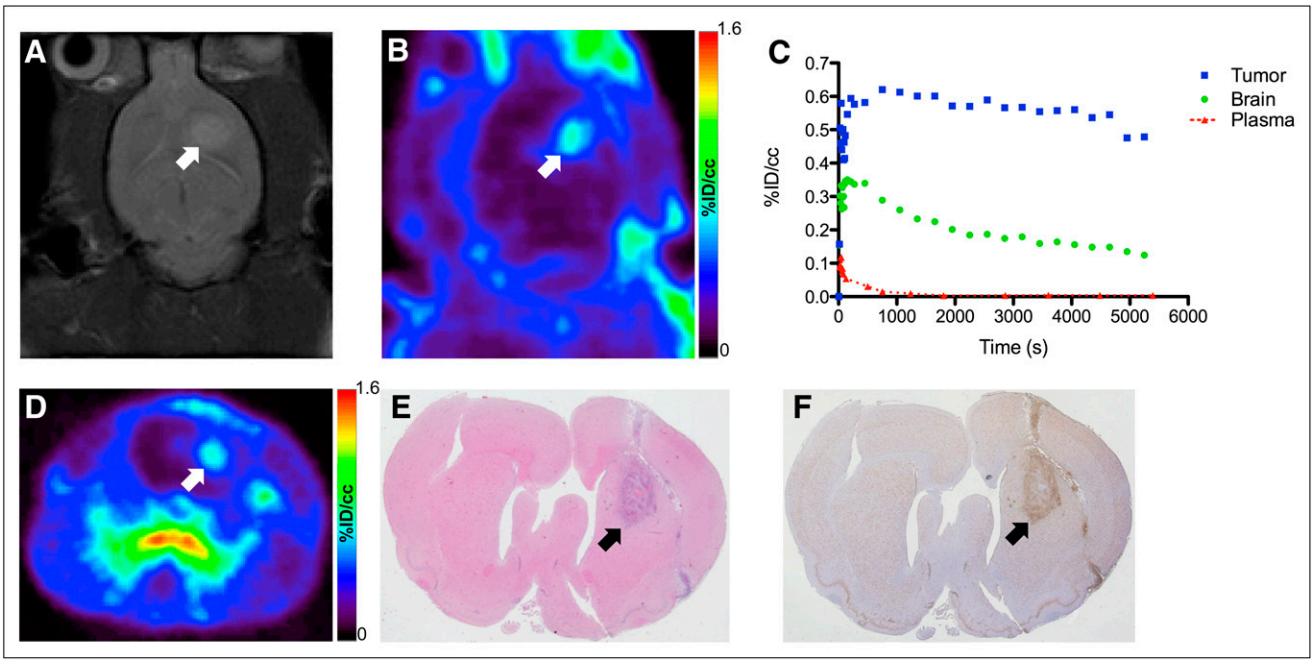

FIGURE 2. (A) T2-weighted MR image of C6 glioma–bearing rat in right brain hemisphere. (B) Coronal PET image obtained from dynamic scan of ^{18}F-DPA-714 PET (summed dynamic scan, 0–90 min). (C) ^{18}F-DPA-714 time–activity curves for tumor (blue), contralateral brain (green), and plasma (red). (D) Transverse PET image obtained from dynamic scan of ^{18}F-DPA-714 PET (summed dynamic scan, 0–90 min). (E) Standard hematoxylin and eosin staining of serial tissue section. (F) Immunohistochemistry analysis of TSPO expression in typical C6 glioma. Tumor location is indicated with arrows in images. %ID/cc = percentage injected dose per cubic centimeter.

than in normal brain. Over the course of imaging, a modest level of radioactivity localized to the skull, indicating defluorination that was later confirmed by HPLC radiometabolite analysis (Table 1; Supplemental Fig. 1 [supplemental materials are available online only at http://jnm.snmjournals.org]). Accumulation of ^{18}F-DPA-714 was observed in the olfactory epithelium and Harderian glands (Supplemental Table 1), which had little impact on brain tumor imaging. Figure 2C illustrates a time–activity curve for tumor, normal brain, and plasma activity for a typical 90-min scan. We found that ^{18}F-DPA-714 washed into both normal brain and tumor tissue rapidly, but washout from tumor tissue was much slower than from normal brain. After the initial spike in plasma activity consistent with tracer injection, ^{18}F-DPA-714 rapidly cleared from the plasma. Imaging-matched brains were processed for staining and immunohistochemistry. Using standard hematoxylin and eosin staining to localize the tumor (Fig. 2E), we found that TSPO immunoreactivity was significantly higher in the tumor than in normal brain (Fig. 2F). Consistent with previous studies of TSPO expression in glioma, TSPO levels measured by immunohistochemistry optical density were 3- to 4-fold higher in tumor than in normal brain tissue (*16,22*). Overall, we found excellent agreement between ^{18}F-DPA-714 accumulation and TSPO levels as measured by immunohistochemistry.

In Vivo Displacement of ^{18}F-DPA-714

To evaluate the in vivo TSPO specificity of ^{18}F-DPA-714, we performed displacement studies in C6-bearing rats using DPA-714. During the dynamic PET study, an excess (10 mg/kg) of DPA-714 was administered intravenously 30 min after the injection of ^{18}F-DPA-714. Summation of the first 30 min of the PET scan before injection of DPA-714 (0–30 min) demonstrated typical uptake characteristics of ^{18}F-DPA-714 (Fig. 3A). However, summation of the final 30 min of the PET scan (60–90 min) demonstrated significant displacement of ^{18}F-DPA-714 in the normal brain and tumor tissue (Fig. 3B). Accordingly, time–activity curve analysis (Fig. 3C) indicated that after injection of DPA-714, tumor activity was reduced approximately 75%, compared with the peak tumor uptake in the animal shown. Over multiple animals with comparatively larger and smaller tumors (n = 4), we observed a mean displacement of peak uptake of greater than 60%. Interestingly, in heterogeneous tumors featuring central necrosis, tracer uptake

TABLE 1
HPLC Radiometabolite Analysis of ^{18}F-DPA-714

Time after injection (min)	Percentage ^{18}F-DPA-714	Percentage ^{18}F-fluoride	Percentage metabolite
2 (n = 7)	95 ± 6.0	2 ± 3.3	3 ± 3.7
12 (n = 7)	68 ± 7.4	13 ± 6.7	19 ± 5.8
30 (n = 7)	44 ± 8.9	37 ± 5.4	19 ± 8.8
60 (n = 7)	27 ± 6.2	50 ± 15.0	23 ± 7.3
90 (n = 5)	22 ± 17.8	64 ± 12.1	14 ± 3.8

Data are mean ± SD.

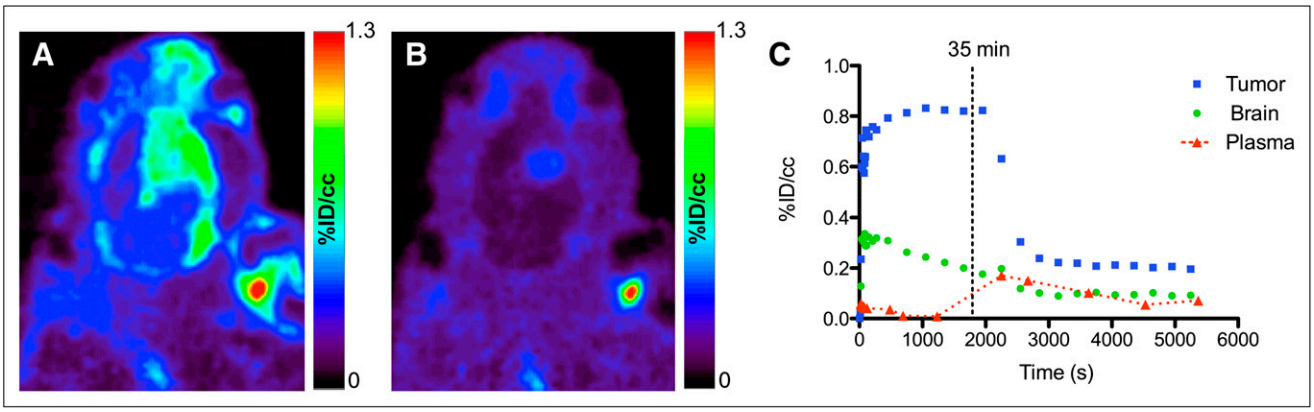

FIGURE 3. In vivo displacement of ^{18}F-DPA-714 in C6 glioma–bearing rat. Relative ^{18}F-DPA-714 uptake before (A) and after (B) intravenous infusion of excess of DPA-714. (C) ^{18}F-DPA-714 time–activity curves generated for tumor (blue), contralateral brain (green), and plasma (red). %ID/cc = percentage injected dose per cubic centimeter.

and specificity appeared greatest in actively proliferating tumor regions. Furthermore, minor, nondisplaceable pooling of ^{18}F-DPA-714 was observed in regions of central necrosis, although levels pooling in these regions tended to be less or similar to uptake in normal, healthy brain.

Direct Comparison of ^{18}F-DPA-714 and ^{18}F-PBR06

To further evaluate the in vivo performance of ^{18}F-DPA-714 in tumor studies, we directly compared the localization and relative tissue uptake of this tracer in C6 glioma–bearing cohorts (n = 2) with that of an aryloxyanilide TSPO PET ligand, ^{18}F-PBR06. A representative study is shown in Figure 4. Tumors were initially localized with T2-weighted MRI (Fig. 4A). Subsequently, serial dynamic PET studies using ^{18}F-DPA-714 (Fig. 4B) or ^{18}F-PBR06 (Fig. 4C) were performed approximately 24 h apart. As shown in Figure 4, both tracers exhibited similar localization to tumor tissue, with only modest retention in the normal brain. Both tracers exhibited similarly rapid clearance from plasma and normal brain. However, time–activity curve analysis illustrated that ^{18}F-DPA-714 was retained in tumor tissue to a somewhat greater extent than ^{18}F-PBR06, which manifested as a modestly higher signal-to-noise ratio (tumor–normal) for ^{18}F-DPA-714 over the last 30 min of the PET scan.

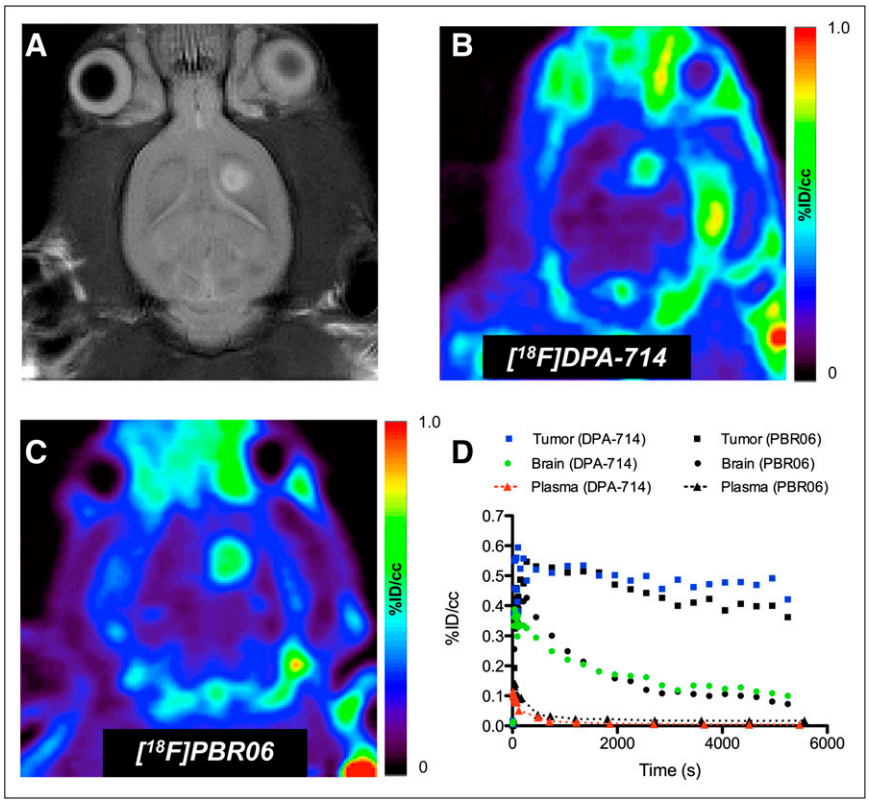

FIGURE 4. Comparison of ^{18}F-PBR06 and ^{18}F-DPA-714 in same glioma-bearing rat. (A) T2-weighted MR image of rat bearing C6 glioma in right hemisphere. (B) ^{18}F-DPA-714 PET image (summed dynamic scan over last 30 min). (C) ^{18}F-PBR06 PET image (summed dynamic scan over last 30 min). (D) ^{18}F-DPA-714 time–activity curves generated for tumor (blue), contralateral brain (green), and plasma (red). For comparison, ^{18}F-PBR06 time–activity curves are shown in black. %ID/cc = percentage injected dose per cubic centimeter.

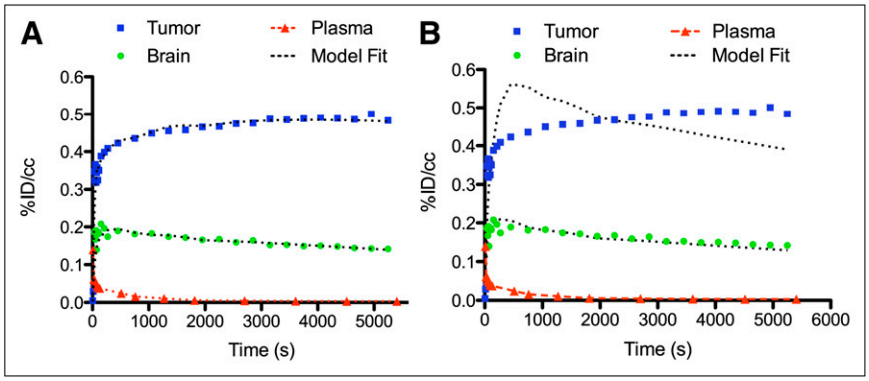

FIGURE 5. Pharmacokinetic model fit of typical ^{18}F-DPA-714 time–activity curves to 3-compartment, 4-kinetic-parameter (A) and 2-compartment, 2-kinetic-parameter (B) models. Time–activity curves for tumor (blue), contralateral brain (green), and plasma (red) are shown with associated model fit. %ID/cc = percentage injected dose per cubic centimeter.

Characterization of ^{18}F-DPA-714 Radiometabolites

Detectable ^{18}F-DPA-714 radiometabolites included free ^{18}F-fluoride (retention time, 2.5 min) and a single radiometabolite more hydrophilic than DPA-714 (retention time, 4.0 min; parent tracer retention time, 5.0 min). As shown in Table 1, immediately after intravenous injection of ^{18}F-DPA-714, the parent tracer accounted for approximately 95% of the whole plasma radioactivity. Subsequently, we observed a steady decrease of parent ligand in the plasma that was roughly equivalent to the increase in free ^{18}F-fluoride over the course of a given imaging study (Supplemental Fig. 1), suggesting that the primary metabolism observed in these studies was defluorination. Levels of the observed hydrophilic radiometabolite were relatively constant beyond the first 10 min of the scan, suggesting that appearance of this species was offset by further metabolism or subsequent clearance.

Compartmental Modeling

To describe the pharmacokinetics of ^{18}F-DPA-714, we evaluated 2-compartment, 2-kinetic-parameter and 3-compartment, 4-kinetic-parameter models. As determined by inspection, fit of the ^{18}F-DPA-714 PET data was superior in the 3-compartment, 4-kinetic-parameter model, and the 2-compartment model was not considered further (Fig. 5). Using the 3-compartment, 4-kinetic-parameter model and the metabolite-corrected AIF, we determined K_1/k_2 and k_3/k_4 for tumor tissue and normal brain (Table 2). Compared with normal brain, tumor tissues tended to exhibit a higher K_1/k_2 and k_3/k_4. Estimation of V_T derived from kinetic parameters and graphical estimation (Fig. 6) were performed both in brain and tumor. Ratios of V_T and percentage injected dose per centimeter cubed between tumor and brain obtained from both methods of estimation were highly similar and yielded statistically significant values that closely mirrored TSPO expression as measured by immunohistochemistry (Table 2).

DISCUSSION

A considerable body of research suggests that TSPO can serve as an important biomarker in oncology. Numerous preclinical and clinical studies have demonstrated prognostic implications associated with elevated TSPO expression in multiple tumor types, including breast (*7,8*), prostate (*9*), oral cavity (*10*), colon (*11–13*), liver (*14*), and brain (*15,16*). The first evidence supporting the hypothesis that TSPO ligands could be used for detection and grading of human brain tumors emerged more than 20 years ago (*16,30,31*), in which autoradiographic (^{3}H-PK 11195) and PET (^{11}C-PK 11195) studies evaluated TSPO expression in experimental models of glioma, postmortem human brain sections (*15,16,30,32*), and patients with glioma (*33*). Although these early studies established the potential utility of TSPO ligands for brain tumor imaging, the most prominent TSPO-selective ligand available at the time, PK 11195, suffered from relatively modest in vivo uptake and attendant low contrast in tumor tissue, compared with normal brain. Furthermore, PK 11195 previously demonstrated considerable levels of nondisplaceable ligand binding in

TABLE 2
Parameter Estimations for ^{18}F-DPA-714 Uptake

Tissue type	K_1/k_2 (mL/g)	k_3/k_4	V_T (mL/g)*	V_T (mL/g)†	%ID/cc
Tumor (n = 11)	6.867 ± 1.226	8.913 ± 1.155	70.033 ± 14.729	57.44 ± 11.742	0.331 ± 0.036
Brain (n = 11)	3.619 ± 0.551	4.024 ± 0.842	15.963 ± 3.566	14.57 ± 2.823	0.088 ± 0.011
P	0.0762	0.0021	0.0017	0.0029	<0.0001

*From kinetic parameters.
†From graphical analysis.
Data are mean ± SEM.

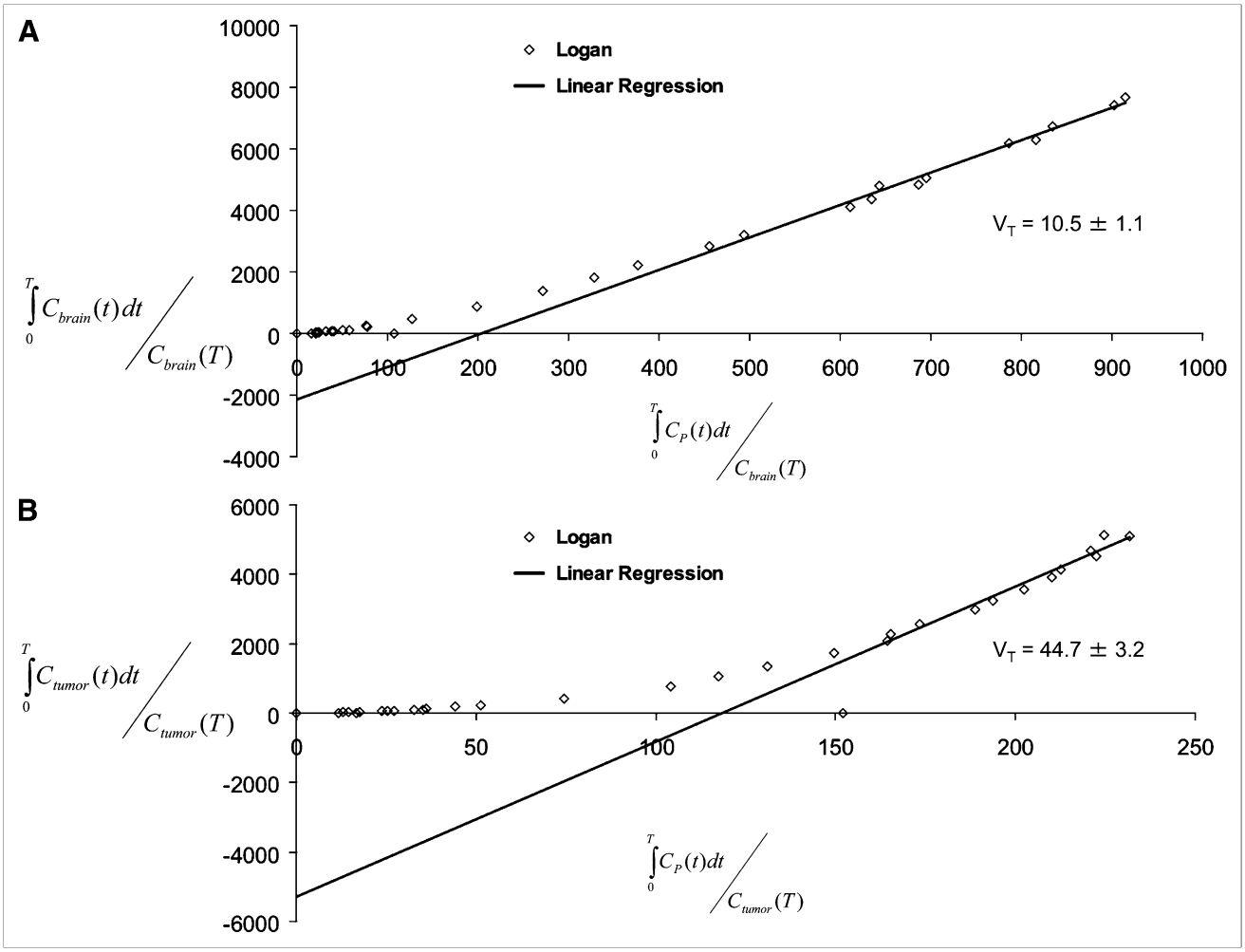

FIGURE 6. Representative graphical analysis of V_T for a subject from this investigation. Fit was performed for normal brain (A) and for tumor (B). Solid gray line = linear regression (start time for linear regression, "t*").

vivo (*33*). Both of these conditions led to ligand uptake that marginally reflected actual TSPO expression levels. These issues recently led us to explore novel TSPO ligands with potentially improved pharmacokinetic properties and in vivo specificity in cancer imaging studies.

For example, we recently reported the first, to our knowledge, preclinical use of an aryloxyanilide-based TSPO ligand, ^{18}F-PBR06, for quantitative assessment of TSPO expression in glioma (*22*). These studies demonstrated that ^{18}F-PBR06 is a highly promising tracer for visualization of brain tumors and quantification of TSPO expression in tumor and surrounding normal tissue. Compared with previous reports using ^{11}C-PK 11195 in brain tumors, ^{18}F-PBR06 demonstrated superior TSPO specificity in vivo, resulting in close agreement between tracer accumulation and TSPO levels.

In this study, we evaluated the pyrazolopyrimidine ^{18}F-DPA-714 in analogous preclinical studies. Like ^{18}F-PBR06, ^{18}F-DPA-714 exhibited uptake that closely mirrored TSPO expression in tumor and normal tissues. Indeed, both tracers exhibited similar accumulation and clearance when compared in the same glioma-bearing animals. Furthermore, ^{18}F-DPA-714 was highly displaceable from normal and tumor tissues. We observed a modest degree of nondisplaceable pooling of ^{18}F-DPA-714 in regions of the tumor that appeared to correlate with central necrosis, although uptake in necrosis was significantly lower than that observed in actively growing portions of the tumor. Analogous to our studies with ^{18}F-PBR06, ^{18}F-DPA-714 time–activity curves derived from tumor and normal brain could be fit to a 3-compartment, 4-kinetic-parameter compartmental model, enabling tracer quantitation (e.g., V_T) in tumor tissue and normal brain. In general, time–activity curves for ^{18}F-DPA-714 uptake in both tumor and normal tissue were remarkably consistent across numerous animals (Supplemental Fig. 2), suggesting the robustness and reproducibility of this imaging approach. Though the aryloxyanilide ^{18}F-PBR06 and pyrazolopyrimidine ^{18}F-DPA-714 both appear to be promising tracers in this preclinical setting, further studies to better characterize determinants such as in vivo metabolism and tissue pharmacodynamics will likely reveal important differences between these two unique scaffolds. We envision that evaluation of these and similar agents

within the context of other solid tumors such as colorectal (*11–13*) and breast (*7,8*) cancers may shed further light on the rational selection of TSPO ligands for cancer imaging.

CONCLUSION

These preclinical studies illustrate the feasibility of using ^{18}F-DPA-714 for visualization of TSPO-expressing brain tumors. Importantly, ^{18}F-DPA-714 appears suitable for quantitative assay of tumor TSPO levels in vivo. Given the relationship between elevated TSPO levels and poor outcome in oncology, these studies suggest the potential of ^{18}F-DPA-714 PET to serve as a novel predictive cancer imaging modality.

DISCLOSURE STATEMENT

The costs of publication of this article were defrayed in part by the payment of page charges. Therefore, and solely to indicate this fact, this article is hereby marked "advertisement" in accordance with 18 USC section 1734.

ACKNOWLEDGMENTS

We gratefully acknowledge Professor Vassilios Papadopoulos of McGill University for the TSPO antibody. Clare A. Osborne, Zou Yue, and Fuxue Xin provided imaging support. This work was supported by funding from the National Cancer Institute (1R01 CA140628, K25 CA127349, 1RC1 CA145138, 1P50 CA128323, and U24 CA126588) and training grants (5R25 CA092043-09, T32 EB003817, and R25 CA136440). No other potential conflict of interest relevant to this article was reported.

REFERENCES

1. Dhermain FG, Hau P, Lanfermann H, Jacobs AH, van den Bent MJ. Advanced MRI and PET imaging for assessment of treatment response in patients with gliomas. *Lancet Neurol.* 2010;9:906–920.
2. van den Bent MJ, Vogelbaum MA, Wen PY, Macdonald DR, Chang SM. End point assessment in gliomas: novel treatments limit usefulness of classical Macdonald's Criteria. *J Clin Oncol.* 2009;27:2905–2908.
3. Papadopoulos V, Baraldi M, Guilarte TR, et al. Translocator protein (18kDa): new nomenclature for the peripheral-type benzodiazepine receptor based on its structure and molecular function. *Trends Pharmacol Sci.* 2006;27:402–409.
4. Papadopoulos V, Lecanu L. Translocator protein (18 kDa) TSPO: an emerging therapeutic target in neurotrauma. *Exp Neurol.* 2009;219:53–57.
5. Diorio D, Welner SA, Butterworth RF, Meaney MJ, Suranyi-Cadotte BE. Peripheral benzodiazepine binding sites in Alzheimer's disease frontal and temporal cortex. *Neurobiol Aging.* 1991;12:255–258.
6. Messmer K, Reynolds GP. Increased peripheral benzodiazepine binding sites in the brain of patients with Huntington's disease. *Neurosci Lett.* 1998;241:53–56.
7. Hardwick M, Fertikh D, Culty M, Li H, Vidic B, Papadopoulos V. Peripheral-type benzodiazepine receptor (PBR) in human breast cancer: correlation of breast cancer cell aggressive phenotype with PBR expression, nuclear localization, and PBR-mediated cell proliferation and nuclear transport of cholesterol. *Cancer Res.* 1999;59:831–842.
8. Carmel I, Fares FA, Leschiner S, Scherubl H, Weisinger G, Gavish M. Peripheral-type benzodiazepine receptors in the regulation of proliferation of MCF-7 human breast carcinoma cell line. *Biochem Pharmacol.* 1999;58:273–278.
9. Fafalios A, Akhavan A, Parwani AV, Bies RR, McHugh KJ, Pflug BR. Translocator protein blockade reduces prostate tumor growth. *Clin Cancer Res.* 2009;15:6177–6184.
10. Nagler R, Ben-Izhak O, Savulescu D, et al. Oral cancer, cigarette smoke and mitochondrial 18kDa translocator protein (TSPO): in vitro, in vivo, salivary analysis. *Biochim Biophys Acta.* 2010;1802:454–461.
11. Maaser K, Grabowski P, Sutter AP, et al. Overexpression of the peripheral benzodiazepine receptor is a relevant prognostic factor in stage III colorectal cancer. *Clin Cancer Res.* 2002;8:3205–3209.
12. Deane NG, Manning HC, Foutch AC, et al. Targeted imaging of colonic tumors in smad3−/− mice discriminates cancer and inflammation. *Mol Cancer Res.* 2007;5:341–349.
13. Maaser K, Hopfner M, Jansen A, et al. Specific ligands of the peripheral benzodiazepine receptor induce apoptosis and cell cycle arrest in human colorectal cancer cells. *Br J Cancer.* 2001;85:1771–1780.
14. Venturini I, Zeneroli ML, Corsi L, et al. Up-regulation of peripheral benzodiazepine receptor system in hepatocellular carcinoma. *Life Sci.* 1998;63:1269–1280.
15. Black KL, Ikezaki K, Toga AW. Imaging of brain tumors using peripheral benzodiazepine receptor ligands. *J Neurosurg.* 1989;71:113–118.
16. Starosta-Rubinstein S, Ciliax BJ, Penney JB, McKeever P, Young AB. Imaging of a glioma using peripheral benzodiazepine receptor ligands. *Proc Natl Acad Sci USA.* 1987;84:891–895.
17. Nagler R, Savulescu D, Krayzler E, Leschiner S, Veenman L, Gavish M. Cigarette smoke decreases salivary 18 kDa translocator protein binding affinity: in association with oxidative stress. *Curr Med Chem.* 2010;17:2539–2546.
18. Galiègue S, Casellas P, Kramar A, Tinel N, Simony-Lafontaine J. Immunohistochemical assessment of the peripheral benzodiazepine receptor in breast cancer and its relationship with survival. *Clin Cancer Res.* 2004;10:2058–2064.
19. Miettinen H, Kononen J, Haapasalo H, et al. Expression of peripheral-type benzodiazepine receptor and diazepam binding inhibitor in human astrocytomas: relationship to cell proliferation. *Cancer Res.* 1995;55:2691–2695.
20. Hardwick M, Rone J, Han Z, Haddad B, Papadopoulos V. Peripheral-type benzodiazepine receptor levels correlate with the ability of human breast cancer MDA-MB-231 cell line to grow in SCID mice. *Int J Cancer.* 2001;94:322–327.
21. Dollé F, Luus C, Reynolds A, Kassiou M. Radiolabelled molecules for imaging the translocator protein (18 kDa) using positron emission tomography. *Curr Med Chem.* 2009;16:2899–2923.
22. Buck JR, McKinley ET, Hight MR, et al. Quantitative, preclinical PET of translocator protein expression in glioma using ^{18}F-*N*-fluoroacetyl-*N*-(2,5-dimethoxybenzyl)-2-phenoxyaniline. *J Nucl Med.* 2011;52:107–114.
23. Tang D, Buck JR, Hight MR, Manning HC. Microwave-assisted organic synthesis of a high-affinity pyrazolo-pyrimidinyl TSPO ligand. *Tetrahedron Lett.* 2010;51:4595–4598.
24. Kozikowski AP, Kotoula M, Ma D, Boujrad N, Tuckmantel W, Papadopoulos V. Synthesis and biology of a 7-nitro-2,1,3-benzoxadiazol-4-yl derivative of 2-phenylindole-3-acetamide: a fluorescent probe for the peripheral-type benzodiazepine receptor. *J Med Chem.* 1997;40:2435–2439.
25. Chauveau F, Van Camp N, Dolle F, et al. Comparative evaluation of the translocator protein radioligands ^{11}C-DPA-713, ^{18}F-DPA-714, and ^{11}C-PK11195 in a rat model of acute neuroinflammation. *J Nucl Med.* 2009;50:468–476.
26. Cleveland WS, Devlin SJ. Locally weighted regression: an approach to regression-analysis by local fitting. *J Am Stat Assoc.* 1988;83:596–610.
27. Innis RB, Cunningham VJ, Delforge J, et al. Consensus nomenclature for in vivo imaging of reversibly binding radioligands. *J Cereb Blood Flow Metab.* 2007;27:1533–1539.
28. Logan J, Fowler JS, Volkow ND, Wang GJ, Ding YS, Alexoff DL. Distribution volume ratios without blood sampling from graphical analysis of PET data. *J Cereb Blood Flow Metab.* 1996;16:834–840.
29. Martín A, Boisgard R, Theze B, et al. Evaluation of the PBR/TSPO radioligand [^{18}F]DPA-714 in a rat model of focal cerebral ischemia. *J Cereb Blood Flow Metab.* 2010;30:230–241.
30. Olson JM, Junck L, Young AB, Penney JB, Mancini WR. Isoquinoline and peripheral-type benzodiazepine binding in gliomas: implications for diagnostic imaging. *Cancer Res.* 1988;48:5837–5841.
31. Cornu P, Benavides J, Scatton B, Hauw JJ, Philippon J. Increase in omega 3 (peripheral-type benzodiazepine) binding site densities in different types of human brain tumours: a quantitative autoradiography study. *Acta Neurochir (Wien).* 1992;119:146–152.
32. Junck L, Olson JM, Ciliax BJ, et al. PET imaging of human gliomas with ligands for the peripheral benzodiazepine binding site. *Ann Neurol.* 1989;26:752–758.
33. Pappata S, Cornu P, Samson Y, et al. PET study of carbon-11-PK 11195 binding to peripheral type benzodiazepine sites in glioblastoma: a case report. *J Nucl Med.* 1991;32:1608–1610.

The Journal of NUCLEAR MEDICINE

Quantitative Preclinical Imaging of TSPO Expression in Glioma Using *N,N*-Diethyl-2-(2-(4-(2-^{18}F-Fluoroethoxy)Phenyl)-5,7-Dimethylpyrazolo[1,5-*a*]Pyrimidin-3-yl)Acetamide

Dewei Tang, Matthew R. Hight, Eliot T. McKinley, Allie Fu, Jason R. Buck, R. Adam Smith, Mohammed Noor Tantawy, Todd E. Peterson, Daniel C. Colvin, M. Sib Ansari, Michael Nickels and H. Charles Manning

J Nucl Med. 2012;53:287-294.
Published online: January 17, 2012.
Doi: 10.2967/jnumed.111.095653

The Journal of Nuclear Medicine is published monthly.
SNMMI | Society of Nuclear Medicine and Molecular Imaging
1850 Samuel Morse Drive, Reston, VA 20190.
(Print ISSN: 0161-5505, Online ISSN: 2159-662X)

SNMMI SOCIETY OF NUCLEAR MEDICINE AND MOLECULAR IMAGING